

# Automated system for surface photovoltage spectroscopy

Cite as: Rev. Sci. Instrum. 92, 013104 (2021); doi: 10.1063/5.0035179

Submitted: 26 October 2020 • Accepted: 27 December 2020 •

Published Online: 22 January 2021



View Online



Export Citation



CrossMark

Y. González,<sup>1,a)</sup> A. Abelenda,<sup>1</sup> O. de Melo,<sup>1</sup> C. Calvo-Mola,<sup>1</sup> L. García-Pelayo,<sup>2</sup> B. J. García,<sup>2</sup> and M. Sánchez<sup>1</sup>

## AFFILIATIONS

<sup>1</sup> Facultad de Física, Universidad de La Habana, San Lázaro y L, Vedado, 10400 La Habana, Cuba

<sup>2</sup> Departamento de Física Aplicada, Universidad Autónoma de Madrid (UAM), 28049 Madrid, Spain

<sup>a)</sup> Author to whom correspondence should be addressed: [yoandris.gonzalez@emt.inrs.ca](mailto:yoandris.gonzalez@emt.inrs.ca). Present address: Institut National de la Recherche Scientifique, Centre Énergie, Matériaux, Télécommunications, 1650 Boulevard Lionel-Boulet, Varennes, Québec J3X 1S2, Canada.

## ABSTRACT

This paper details the development of a lab-made experimental setup for surface photovoltage spectroscopy (SPS) measurements using an open-source and Arduino® microcontroller to control a monochromator and some off-the-shelf electronic components. The experimental setup is interfaced to a computer, where LabVIEW® based software manages system control and data acquisition. We also report the design of a compact sample holder, simple and easy to manufacture and handle. Results of the application of SPS to the characterization of MoO<sub>3</sub> thin films and semiconductor laser structures are presented to validate the performance of the setup, highlighting the effectiveness of SPS for the characterization of semiconductor materials and devices.

Published under license by AIP Publishing. <https://doi.org/10.1063/5.0035179>

## I. INTRODUCTION

The analysis of surface photovoltage (SPV) as a function of the wavelength of incident light is known as surface photovoltage spectroscopy (SPS).<sup>1</sup> In the last few years, this technique has become an important semiconductor characterization tool because of its simplicity and its advantages when compared to other spectroscopic techniques, such as photoluminescence (PL) and photoreflectance (PR), which generally require the use of cryogenic temperatures and different laser sources. Moreover, as SPS is a contactless and nondestructive technique in which samples do not require any special preparation, SPS measurements can be carried out in practically any ambience. For specific details about the technique and its applications, see review articles.<sup>2,3</sup>

Optical excitation of semiconducting samples modifies the concentration of charge carriers on their surface and consequently the surface potential barrier; SPS relies on measurement of the resulting light-induced variation of this surface potential barrier as a function of incident wavelength. SPV is defined as the difference between the surface potential barrier ( $V_s$ ) under illumination and in the dark,

$$\text{SPV} = V_s(\text{light}) - V_s(\text{dark}) \quad (1)$$

SPS has been used traditionally to study the electronic properties of surfaces and to extract basic semiconductor parameters such as bandgap energy, conductivity type, and the diffusion length of minority carriers. In addition, it is also suitable to extract information about buried interfaces in multilayered structures, allowing to obtain the complete structure's band profile.<sup>2</sup> SPV measurements are customarily carried out in the photovoltaic industry to determine the minority carrier diffusion length in silicon wafers, based on Goodman's approach.<sup>4</sup>

As experimental methods and algorithms used for data analysis have been developed, SPS applications expanded further. Today, the technique is used for the study of a wide spectrum of low dimensional semiconductor systems and materials, including III-nitrides, Si-based nanostructures, porous semiconductors,<sup>5</sup> and transition metal oxide layers.<sup>6</sup> Recently, SPS has also demonstrated its potential in the evaluation of important parameters in full devices, such as solar cells<sup>7</sup> and laser diodes.<sup>8</sup> The combination of surface photovoltage measurements with atomic force microscopy provided a

powerful tool to measure SPV surface maps<sup>9</sup> widely used at present in the analysis of semiconductor structures.<sup>10,11</sup>

Usually, SPV measurements are carried out in two different ways: the Kelvin probe (KP) and the metal–insulator semiconductor (MIS) configuration;<sup>2</sup> both are capacitive pick-up techniques. In the KP arrangement, the sample is placed between two electrodes forming a parallel plate capacitor; one is held stationary while the other, the KP, is vibrated in a periodic way. The KP is made of a metallic grid or a semitransparent conductor, and a constant illumination is used. As the electrode vibrates, the distance between the probe and the sample varies, changing the device capacitance and the capacitor charge; hence, the current in the external circuit changes periodically. Thus, the contact potential difference (CPD) between the two electrodes is detected by determining the external voltage that must be applied to discharge the capacitor and nullify the external current.<sup>2,5</sup> The difference between the CPD values in the dark and under illumination is the SPV signal.

Under the alternative MIS geometry, both electrodes are fixed, while SPV is measured via a high-impedance buffer using frequency-modulated (chopped) light as the excitation source, as shown in Fig. 1. The sample is ohmically in contact with the back electrode, and the top semitransparent conductive electrode is separated from the sample by air or another insulator.<sup>5</sup> Periodic generation of excess carriers by electron–hole pair creation and their consequent redistribution induces a periodic SPV signal. A simplified version of the MIS method, in which the semitransparent electrode is kept in soft contact with the sample, is the so called “soft contact” mode introduced by Datta *et al.*<sup>12</sup> The authors demonstrated a strong increase in the measured SPV signal as compared to the conventional method. This soft contact mode is used in this work.

Presently, commercial equipment for Kelvin probe SPV measurements is unaffordable for many research groups. This situation can be overcome by developing homemade experimental setups. This do-it-yourself approach (DIY), besides the obvious economic advantage, has the benefit of flexibility since we can build exactly what is needed for our particular lab process depending on the desired output and the equipment available.

Some other home-made SPV experimental setups have been reported previously, however no details about their automation were shown. For example, in Ref. 13, authors present an automated setup

for the measurement of SPV spectra in a Kelvin probe arrangement;<sup>13</sup> in addition, in Ref. 14, authors presented an original Kelvin probe design.<sup>14</sup> An SPV setup in the MIS operation mode was also reported recently.<sup>15</sup>

This paper reports the design of a homemade experimental setup for SPS studies as a simple solution to more expensive commercial instruments. The control unit based on an Arduino® Leonardo board is dedicated to the automation of monochromator scans. The overall system is controlled by a computer using LabVIEW® based software to allow whole experiment automation. A sample holder specially designed for SPV measurements is also proposed. The performance of the system is demonstrated by presenting original results on the characterization of semiconductors structures and devices.

## II. EXPERIMENTAL DETAILS

In the MIS approach for SPV measurement, the light coming from a lamp passes through a monochromator, being chopped at a moderate frequency and focused onto the sample surface, while the SPV signal is measured by a lock-in amplifier. Our system comprises an MDP-23 LOMO grating monochromator with a spectral range from 200 nm to 1200 nm, an optical chopper (Thorlabs MC2000), a sample holder specially designed to carry out the measurements, and a lock-in amplifier (Stanford Research Systems, model 830) that is computer-controlled by an RS232 port.

The control unit based on an Arduino Leonardo board was developed to manage the rotation of the diffraction grating of the monochromator. The whole system is automated and controlled by a personal computer (PC). The experimental setup is sketched in Fig. 2, which describes the interconnection of the different system components.

### A. Monochromator automation

The MDR-23 monochromator was originally equipped with a stepper motor mechanically connected to the diffraction grating and an obsolete control system (ShDR-71), which makes its integration with modern electronics difficult. The original motor was replaced by a 23KM-K042 stepper motor, with a full step angle of 1.8° and 200 steps per lap, while the control unit was substituted by an open-source electronics Arduino Leonardo platform based on the ATmega32u4 microcontroller<sup>16</sup> (5 V power supply, 16 MHz clock frequency, 32 KB of flash memory for code – 4 KB used by bootloader and 1 KB of EEPROM for system parameters). The Arduino Leonardo board also has 20 digital input/output pins and a built-in USB connection for communications to the host computer. For additional information on the hardware, see the Arduino site.<sup>17</sup>

The stepper motor was connected to the Arduino board via a stepper motor driver using the outputs 9–12. The microcontroller sends to the stepping motor driver the pulse sequence needed to set the rotation of the diffraction grating in the desired direction, allowing the automation of the monochromator and the integration with other components of the experimental setup. Figure 3 shows the block diagram of the designed monochromator control unit, while the electric circuit is sketched in Fig. 4. Similar automation works

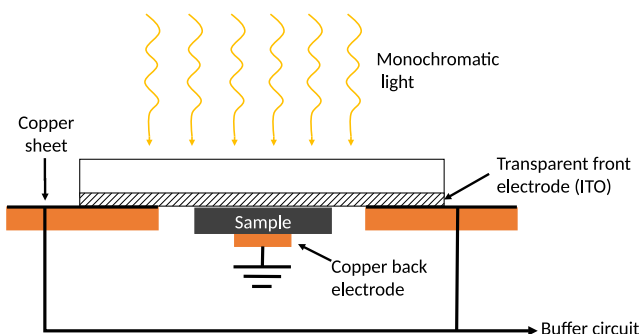
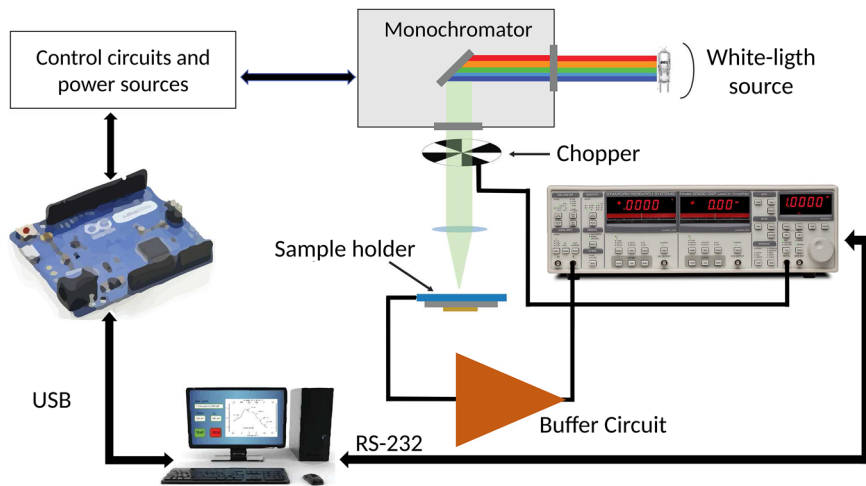


FIG. 1. Transversal view of the configuration for SPV measurements under the MIS arrangement.



**FIG. 2.** Schematic of the automated setup developed for surface photovoltaic spectroscopy measurements.

on other spectrometers using an Arduino Uno<sup>18</sup> and Atmega8535 microcontroller<sup>19</sup> have been reported by other authors.

The end sensor shown in Fig. 3 is placed at both end-limit positions of the diffraction grating as a stop switch to prevent the motor from rotating the gratings beyond their limits.

### B. Arduino Leonardo programming

The code was written and uploaded to the board using the open-source Arduino software (IDE).<sup>17</sup> The control unit was calibrated to determine the number of pulses required to produce the desired variation in wavelengths; in our case, we observed that a 90° rotation of the stepper motor produces a 0.1 nm variation in the wavelength. The sequence to move the stepper motor was generated using the functions provided in the library stepper.h.<sup>20</sup> The code running on the microcontroller receives the angle and

direction of rotation as instructions from the main program (see below) executed on the computer. A feedback signal is sent back at the end of the moving execution. The microcontroller program also checks whether the end-limit switches have been reached, sending an error message if reached. The main program synchronizes the movement of the diffraction grating and the voltage measurements of the lock-in amplifier.

### C. Sample holder

In the MIS soft contact measurement method,<sup>12</sup> the sample holder plays an important role. We report the design of a suitable and simple sample holder, see Fig. 5, made of a piece of a single-sided copper printed circuit board, to which a 1 cm<sup>2</sup> square window was opened. The top electrode is an indium-tin-oxide (ITO) coated slide of soda lime glass (fused silica was also used for materials in

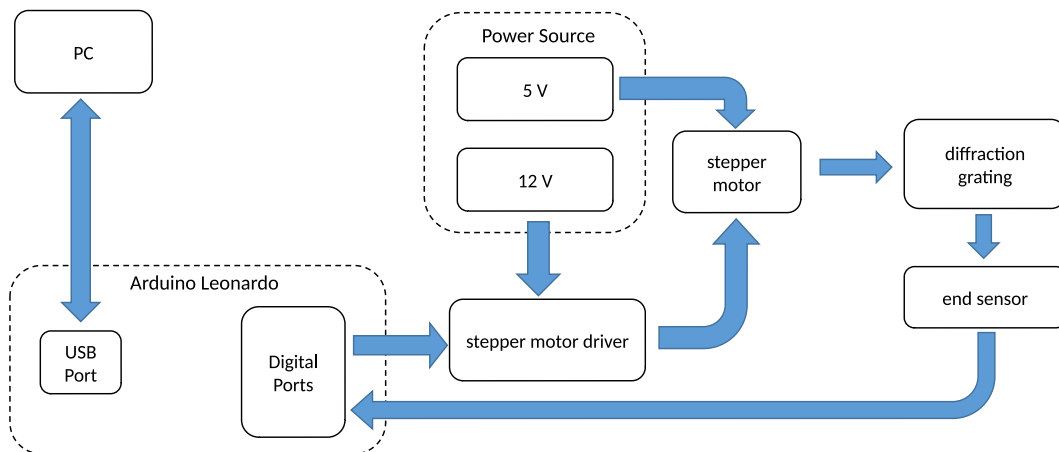


**FIG. 3.** Block diagram of the monochromator control unit.

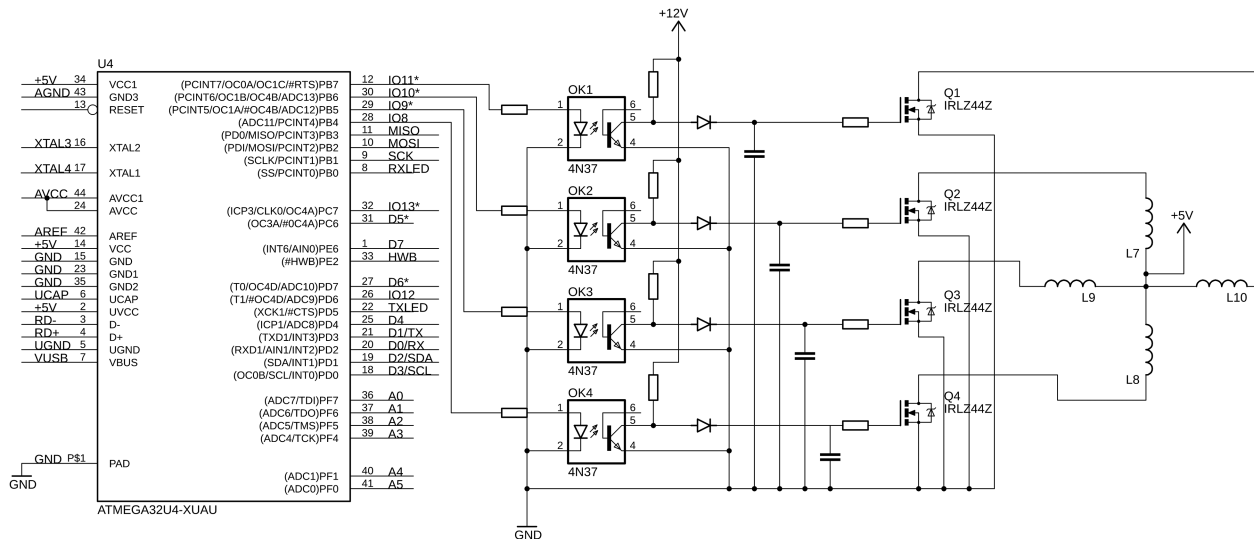


**FIG. 4.** Diagram of the control unit and power circuit. The microcontroller ATmega32U4 It is powered by an external power supply (+5 V), and +12 V is needed for the driver of the stepper motor.

which UV excitation is demanded) fixed to the conductive side of the board with a clip. The ITO-coated side of the glass is fixed upside down onto the window, making electric contact with the copper on the board, serving both as a mechanical holder of the sample and as a front transparent electrode. In the opposite side of the board, a flexible copper clip gently presses the sample against the ITO film, acting as the back electrode. Top and bottom electrodes are properly coupled to a BNC connector. In this way, the sample is sandwiched between the isolated front and back electrodes. The sample holder is affixed onto an x-y positioner allowing the alignment of the sample

with the incident light beam. This sample holder allows for an easy placement and fast exchange of samples.

The ITO-coated top electrode gently touches the sample surface in a very small region while being illuminated by chopped light. The copper back contact is covered with conducting silver paste to improve the electrical conduction.

The modulated light beam impinging onto the sample generates the SPV signal, which is picked up by a wire soldered to the sample holder. It goes through to a buffer circuit based on a JFET-input operational amplifier LF411 with a very high input impedance ( $10^{12} \Omega$ ) configured as a unity-gain voltage follower<sup>21</sup> and then is detected by the lock-in amplifier. Figure 6 shows the schematic of the buffer circuit used to couple the sample with the lock-in amplifier. The high input impedance of the operational amplifier

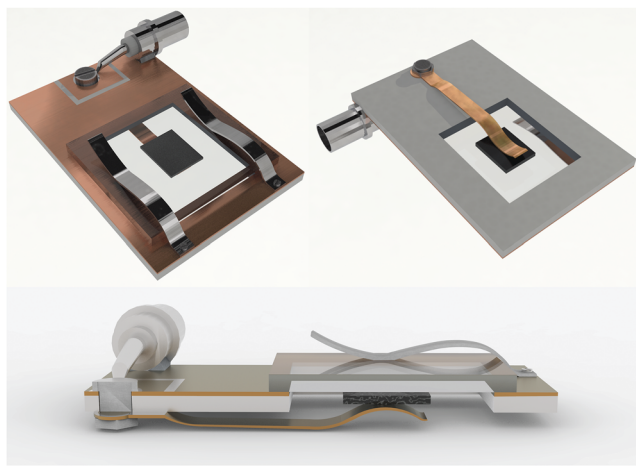


**FIG. 5.** Schematics of the top (left) and bottom (right) view of the sample holder. A cross section image is shown below.

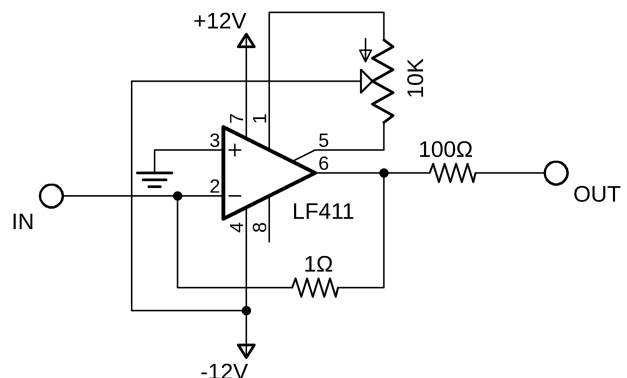


**FIG. 6.** Circuit schematic of the unity gain amplifier.

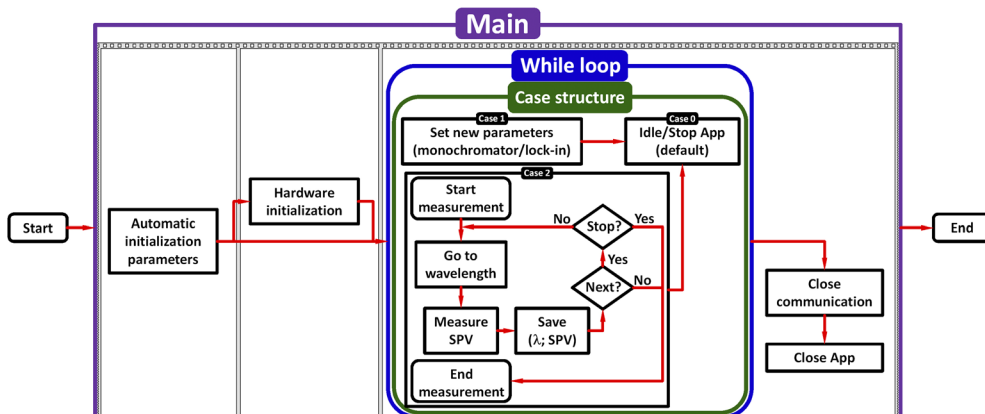


FIG. 7. Flowchart for the software architecture.

(LF411 or similar) is the key reason for having a nearly insulated contact at the top sample surface during SPV measurements. The  $1\ \Omega$  feedback resistor may be substituted by a cable or wire, while the  $100\ \Omega$  resistor is included only as an output short circuit protection. The  $10\ K$  variable resistor is used for balance or offset null.

#### D. System control software

LabVIEW based software for system control and data acquisition was developed, using the LabVIEW 13.0.1 software package. The software architecture is shown in Fig. 7.

The virtual instrument (VI) allows the control of the monochromator through Arduino's own USB connector and the lock-in via RS232 serial communication protocol. The "state machine" technique was used to integrate the main program modules, the monochromator control, the lock-in amplifier control and user interface. The VI is used to set measurement parameters such as sample name, measurement range, pass, gain, chopping frequency, and diffraction grating. The program shows the acquisition of the SPV spectrum in real time. At the end of the experiment, a text file with the experimental results can be easily exported from the application. The LabVIEW application builder module was used to create a stand-alone end-use application, allowing users to easily operate the application without any prior knowledge of LabVIEW. Although this VI is intended for our specific instruments, it could be easily adapted, for instance, to similar equipment from other suppliers.

### III. RESULTS

A standard tungsten lamp was used as the light source in this work, whose light intensity, and photon flux, exhibit a spectral dependence on photon energy close to a black body spectrum; therefore, the photon flux is not constant during measurements. The spectral response of the spectrometer diffraction grating is neither constant on wavelength, also introducing additional photon flux

variation during scanning. These variations may introduce fake, but smooth, features in SPV spectra; thereby, some correction procedures should be used to ensure that features observed in the spectra do not come from the lamp. Unfortunately, in SPV measurements, standard procedures widely used in other spectroscopies, such as normalization of the SPV signal on the lamp's (and grating) spectral dependence, are not fully justified since the dependence of the SPV on the photon flux is sub-linear. A detailed analysis on this subject can be found in Ref. 2. To overcome this difficulty, we compared every spectral feature with the calibrated photon flux spectrum to rule out instrumental artifacts and to ensure the features reported do not come from the lamp in any way. The SPV spectrum derivative technique also helps reject the influence of these smooth features associated with a non-constant photon flux variation during scanning.

#### A. SPS of $\text{MoO}_3$ thin films

Experiments with the developed system were conducted to investigate the energy transitions of molybdenum trioxide ( $\text{MoO}_3$ ) thin films grown onto silicon substrates. Details of the preparation of the samples were reported elsewhere.<sup>6</sup>  $\text{MoO}_3$  belongs to the family of transition metal oxides (TMOs), and is a promising material for applications in electrochemical energy storage devices, gas sensors, battery electrodes, as well as charge injection or extraction layers in solar cells and catalysts, among others.<sup>22</sup>

A typical SPV spectrum is shown in the left plot of Fig. 8. It is worth mentioning that, in SPS, the energies of the relevant electronic transitions may be identified as the inflection points in the SPV spectrum. Following this criterion, three features located at 3.05 eV, 2.41 eV, and 2.0 eV can be clearly observed. These features are better shown in the right plot of Fig. 8, in which the numerical derivative of the spectrum, obtained as  $d[E \cdot \text{SPV}(E)]/dE$ , vs the incident photon energy  $E$  is shown. The 3.05 eV feature corresponds to a  $\text{MoO}_3$  near bandgap transition, while transitions at 2.41 eV and 2.0 eV may be attributed to the presence of different defect states inside the bandgap (such as oxygen vacancies and Mo interstitial

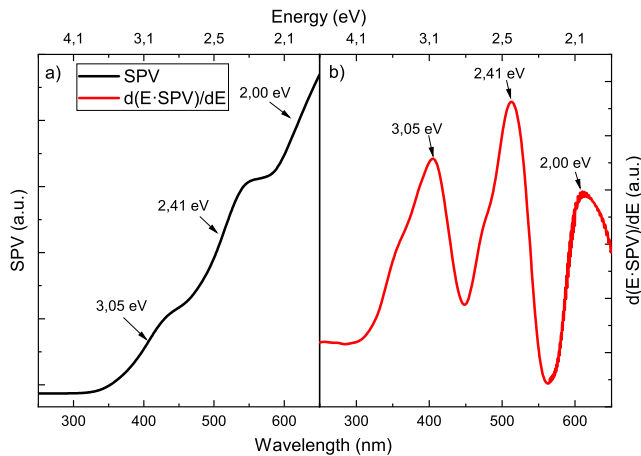


**FIG. 8.** (a) Surface photovoltaic spectra of a  $\text{MoO}_3$  sample. (b) First derivative of the SPV signal. Features corresponding to near bandgap transition (3.05 eV) and those coming from bandgap defect states at 2.41 eV and 2.0 eV are clearly identified.

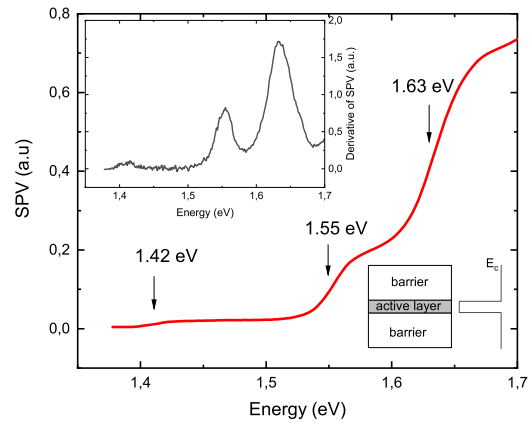


**FIG. 9.** SPV spectrum measured for an AlGaAs laser. Peaks corresponding to the GaAs substrate, AlGaAs active region, and barriers can be clearly differentiated. Inset: derivative SPV spectra. In the right bottom corner, schematics of the structure's active region and conduction band energy diagram are depicted.

sites), as it has been previously reported from photoluminescence studies.<sup>23,24</sup>

Oxygen vacancies in  $\text{MoO}_3$  films have been demonstrated to play a significant role in modifying its electronic and optical properties, being beneficial for applications such as sensors and solar cells; it is also speculated they are responsible for the electrochromic response observed in this material.<sup>25</sup> Moreover, the oxygen vacancy defect band inside the bandgap is expected to allow for efficient hole extraction in solar cells. SPS provides a new perspective to determine the presence of intrinsic or induced vacancies in the films, which is hard to be determined by other methods. We assume that observed transitions at 2.41 eV and 2.0 eV are probably related with oxygen vacancy defects.

### B. SPS of AlGaAs laser structures

As previously reported, we have demonstrated the effectiveness of SPS to obtain the structure's band diagram in laser diode structures.<sup>8</sup> The core of a conventional AlGaAs edge-emitting laser structure consists of several  $\text{Al}_x\text{Ga}_{1-x}\text{As}$  layers of different compositions, thicknesses, and doping levels. The active region is surrounded by barriers with a higher aluminum composition to provide carrier confinement. Figure 9 shows the SPV spectrum of such a laser structure obtained using the system reported in this work.

In the figure, the signature of the GaAs substrate (1.42 eV), the  $\text{Al}_{0.14}\text{Ga}_{0.86}\text{As}$  active region (1.55 eV), and  $\text{Al}_{0.3}\text{Ga}_{0.7}\text{As}$  barriers (1.63 eV) are clearly seen. In the inset, a plot of the numerical derivative of the spectrum is also included. Also shown are schematics of the laser structure active region and the conduction band energy diagram. SPS measurements were performed to the fully metallized structure, proving this technique is effective in getting information about constituent layers inside the heterostructure without the necessity of etching away the individual layers.

## IV. CONCLUSIONS

We have developed an accurate system that can be easily used to perform SPS studies. The control unit is based on an Arduino Leonardo microcontroller board and some standard electronic components. LabVIEW based software allowing automation of the experiments was developed (the program code and detailed instructions are available from the authors on request). A compact, simple, and easy to handle sample holder design for carrying out the measurements is presented. A buffer circuit based on a high-impedance operational amplifier allows us to acquire reliable SPV signals. The performance of the system is demonstrated by presenting original results for the characterization of materials and devices such as  $\text{MoO}_3$  thin films and semiconductor laser diodes. The developed setup may also be used to perform other spectroscopic measurements, even using some “old generation” or legacy spectrometers with high operational and metrological parameters that could be automated and updated in this way.

## DATA AVAILABILITY

The data that support the findings of this study are available from the corresponding author upon reasonable request.

## REFERENCES

- H. C. Gatos and J. Lagowski, *J. Vac. Sci. Technol.* **10**, 130 (1973).
- L. Kronik and Y. Shapira, *Surf. Sci. Rep.* **37**, 1 (1999).
- D. K. Schroder, *Meas. Sci. Technol.* **12**, R16 (2001).
- A. M. Goodman, *J. Appl. Phys.* **32**, 2550 (1961).
- D. Cavalcoli, B. Fraboni, and A. Cavallini, *Semiconductors and Semimetals* (Academic Press, Inc., 2015), pp. 251–278.
- O. De Melo, V. Torres-Costa, A. Climent-Font, P. Galán, A. Ruediger, M. Sánchez, C. Calvo-Mola, G. Santana, and V. Torres-Costa, *J. Phys.: Condens. Matter* **31**, 295703 (2019).

- <sup>7</sup>V. W. Bergmann, Y. Guo, H. Tanaka, I. M. Hermes, D. Li, A. Klasen, S. A. Bretschneider, E. Nakamura, R. Berger, and S. A. L. Weber, *ACS Appl. Mater. Interfaces* **8**, 19402 (2016).
- <sup>8</sup>Y. González, A. Abelenda, and M. Sánchez, *J. Phys.: Conf. Ser.* **792**, 012021 (2017).
- <sup>9</sup>Y. Rosenwaks, S. Saraf, O. Tal, A. Schwarzman, T. Glatzel, and M. C. Lux-Steiner, *Scanning Probe Microscopy* (Springer, New York, 2007), pp. 663–689.
- <sup>10</sup>Y. Huang, A. Gheno, A. Rolland, L. Pedesseau, S. Vedraine, O. Durand, J. Bouclé, J. P. Connolly, L. Etgar, and J. Even, *Opt. Quantum Electron.* **50**, 41 (2018).
- <sup>11</sup>M. J. Shearer, M.-Y. Li, L.-J. Li, S. Jin, and R. J. Hamers, *J. Phys. Chem. C* **122**, 13564 (2018).
- <sup>12</sup>S. Datta, S. Ghosh, and B. M. Arora, *Rev. Sci. Instrum.* **72**, 177 (2001).
- <sup>13</sup>K. Germanova, L. Nikolov, and C. Hardalov, *Rev. Sci. Instrum.* **60**, 746 (1989).
- <sup>14</sup>E. Beyreuther, S. Grafström, and L. M. Eng, *Sensors* **18**, 4068 (2018).
- <sup>15</sup>V. Donchev, *Mater. Res. Express* **6**, 103001 (2019).
- <sup>16</sup>Microchip Technology, Inc., <https://www.microchip.com/wwwproducts/en/atmega32u4>, 2020.
- <sup>17</sup>Arduino, <https://www.arduino.cc/>, 2020.
- <sup>18</sup>T. Zinchenko, E. Pecherskaya, P. Golubkov, D. Artamonov, G. Kozlov, and Y. Shepeleva, *Procedia Computer Science* (Elsevier B.V., 2020), pp. 477–486.
- <sup>19</sup>S. P. Kraminin, E. M. Zobov, and M. E. Zobov, *J. Appl. Spectrosc.* **82**, 307 (2015).
- <sup>20</sup>M. Margolis, *Arduino Cookbook* (O'Reilly Media, Inc., 2011), ISBN: 9781449313876.
- <sup>21</sup>Texas Instruments, LF411 Low Offset, Low Drift Dual JFET Input Operational Amplifier, 1998.
- <sup>22</sup>I. A. de Castro, R. S. Datta, J. Z. Ou, A. Castellanos-Gomez, S. Sriram, T. Daeneke, and K. Kalantar-zadeh, *Adv. Mater.* **29**, 1701619 (2017).
- <sup>23</sup>N. Illyaskutty, S. Sreedhar, G. Sanal Kumar, H. Kohler, M. Schwotzer, C. Natzeck, and V. P. M. Pillai, *Nanoscale* **6**, 13882 (2014).
- <sup>24</sup>A. Boukhachem, M. Mokhtari, N. Benameur, A. Ziouche, M. Martínez, P. Petkova, M. Ghamnia, A. Cobo, M. Zergoug, and M. Amlouk, *Sens. Actuators, A* **253**, 198 (2017).
- <sup>25</sup>C. Z. Chen, Y. Li, and X. D. Tang, *Physica B* **481**, 192 (2016).